Supplementary Information:

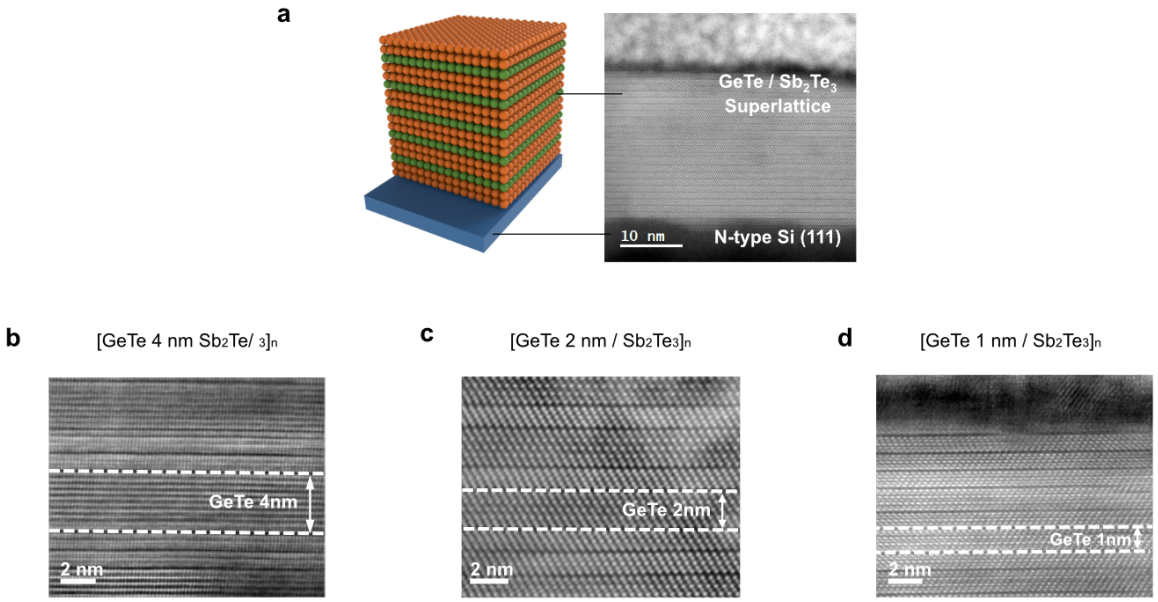

Fig. S1 | HAADF image of single-crystal $[Sb_2Te_3/\ GeTe]_5/\ Sb_2Te_3$ 10 nm SL films with a freely controlled GeTe thickness of a) 4 nm, b) 2 nm, and c) 1 nm. To evaluate the phase-change process, a single-crystal with $[Sb_2Te_3/\ GeTe]_5/\ Sb_2Te_3$ 10 nm SL films were grown on n-type Si (111) using MBE. A thin film was successfully fabricated with a GeTe/Sb_2Te_3 SL structure with freely controlled GeTe thickness from 1 to 4 nm. As shown in Fig. S1a, the structural properties of the thin film were confirmed with a uniform thin film and an alternate structure composed of Sb_2Te_3 and GeTe. Since the direction of the seed layer, Sb_2Te_3, is aligned with the [0 0 3] plane, the directions of the GeTe and Sb_2Te_3 deposited thereon were also satisfactorily aligned.

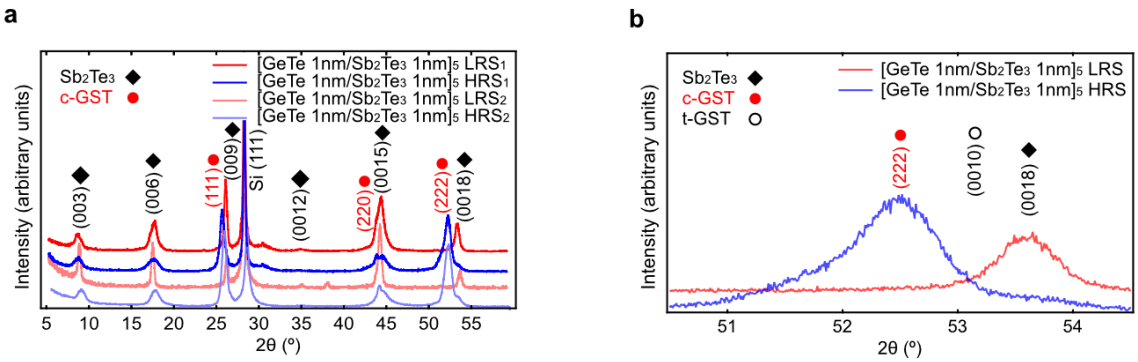

Fig. S2 | a) XRD θ-2θ scan in LRS_1, laser pulse-induced HRS_1, annealing LRS_2, re-laser pulse-induced HRS_2 in $[Sb_2Te_3$ (1 nm)/ GeTe (1 nm)$]_5$/ Sb_2Te_3 10 nm SLs. b) XRD θ-2θ scan of the LRS and HRS in the 50–55 ° range. To study the phase-change process in a GeTe/Sb_2Te_3 SL structure through the transition between crystalline structures, the laser pulse-induced first stable state (LRS) to second stable state (HRS) phase transformation was executed using the in-situ laser pulsing system. Sample oxidation was effectively prevented, resulting in secure experimentation to obtain surface-sensitive phase information without external factors using the in-situ laser pulsing system. Additionally, it was confirmed that the resistance change was reversible during the annealing process. The reversible phase change through laser pulsing and annealing was additionally confirmed by XRD measurements. The c-GST and t-GST peaks corresponded to fcc (222) (52.4°) and hcp (0010) (53.2°), respectively. The reference XRD peaks were adapted from Behrens, M. et al.[27] Because of the similarity between the fcc and hcp structures, the XRD peaks were similar; however, the GST peak in the HRS was consistent with fcc (222) (52.4°) rather than hcp (0010) (53.2°).

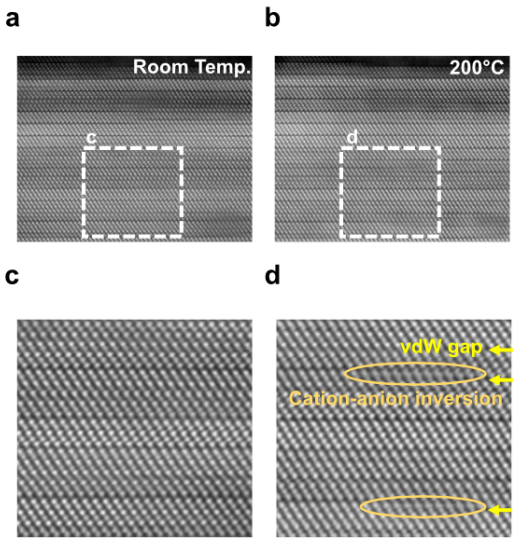

Fig. S3 | HAADF-STEM image of a) laser irradiated $[Sb_2Te_3$ (1 nm)/ GeTe (1 nm)$]_5$/ Sb_2Te_3 10 nm SLs film and b) SL film heat-treated after laser pulsing at the same location. A close comparison of the white dash line boxes in Fig. Sa and Fig. Sb revealed that bilayer defects marked by orange ellipses were formed through the transition. Tracing the change in images before and after the phase change at the identical region during in-situ annealing, allowed for the successful observance of the vdW gap reconfiguration occurring during the heat treatment process. Additionally, the gap in the LRS state resulted from the Ge atom rearrangement in the HRS during the annealing process, i.e., the central Ge layer of the GST block may migrate to the adjacent layer, thus forming a gap.

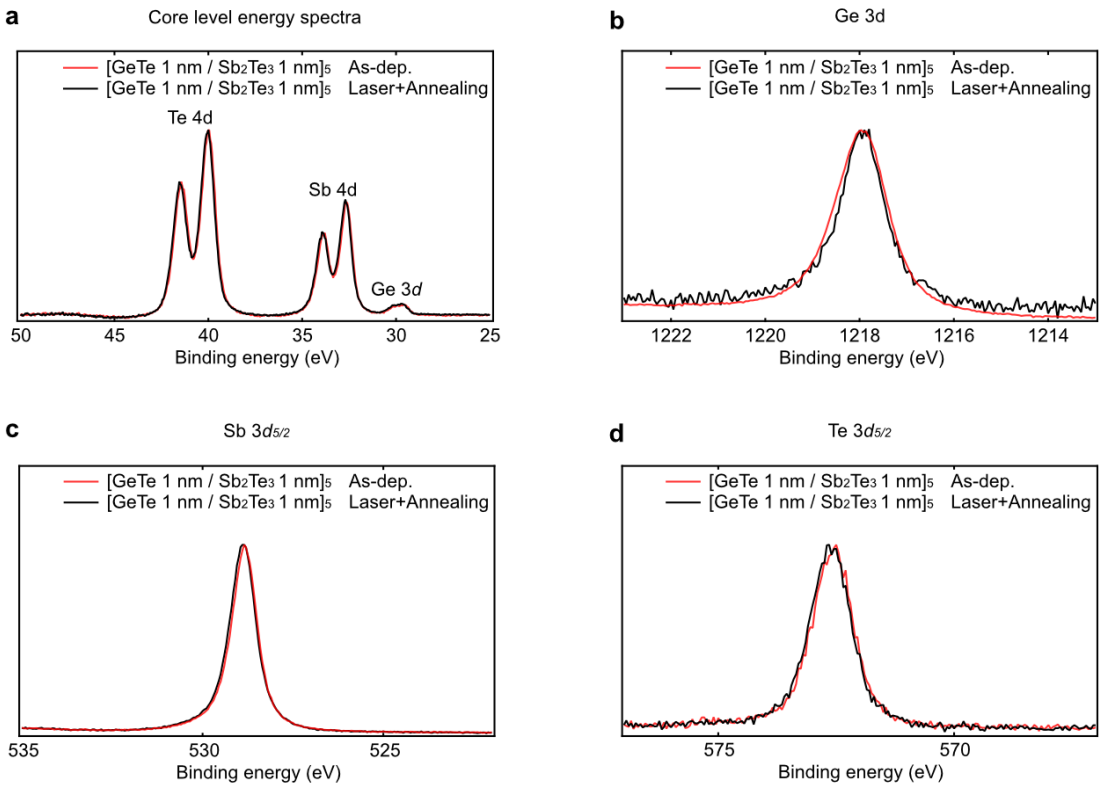

Fig. S4 | a) Shallow core-level energy spectra of the LRS and HRS. Deep core-level spectra of b) Ge $2p_{3/2}$, c) Sb$3d_{5/2}$ and d) Te $3d_{5/2}$. MBE as-deposited iPCM and iPCM with laser pulsing and annealing processes were compared to determine whether the optical laser pulsing phase change was reversible in the chemical state. We confirmed that the local structure around the Ge atoms, which differed during the phase change to HRS in XPS (Fig. S4), returned to their original states through heat treatment.

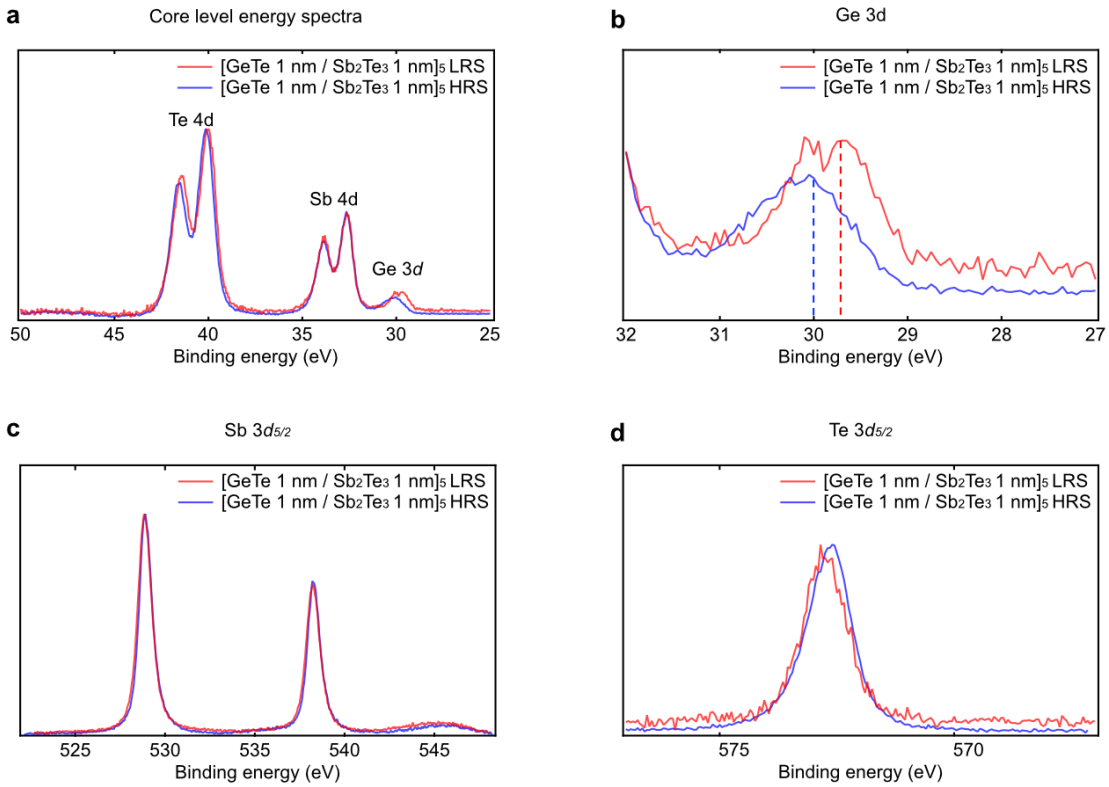

Fig. S5 | a) Shallow core-level energy spectra of the LRS and HRS. Deep core-level spectra of b) Ge 3d, c) Sb3$d_{5/2}$, and d) Te 3$d_{5/2}$. In the core-level energy state, the 29.7 and 30.0 eV chemical binding energies correspond to the octahedral ($Ge^{octahedral}$) and distorted octahedral ($Ge^{distorted\ octahedral}$) structures, respectively. The Ge atoms in the reset state showed an enhanced intensity of $Ge^{distorted\ octahedral}$. The intensity of $Ge^{distorted\ octahedral}$ in the reset state was enhanced, while that of $Ge^{octahedral}$ decreased after the laser pulsing phase change, which was an identical change to the Ge chemical state of the GST alloy local structure. The change in the chemical bonding with Ge represented the structural modulation in iPCM between the distorted octahedral and octahedral structures during the phase-change process. Despite the phase change between the two crystalline states in the SL structure, the chemical bonding change caused by local structure transition was similar to the GST alloy resulting from the Ge local structure, which was the phase change between the amorphous and crystalline states.

Conversely, there was minimal change in the local structures near the Sb and Te atoms during the phase transition, resulting in insignificant Sb and Te $3d_{5/2}$ orbital peak shifts.

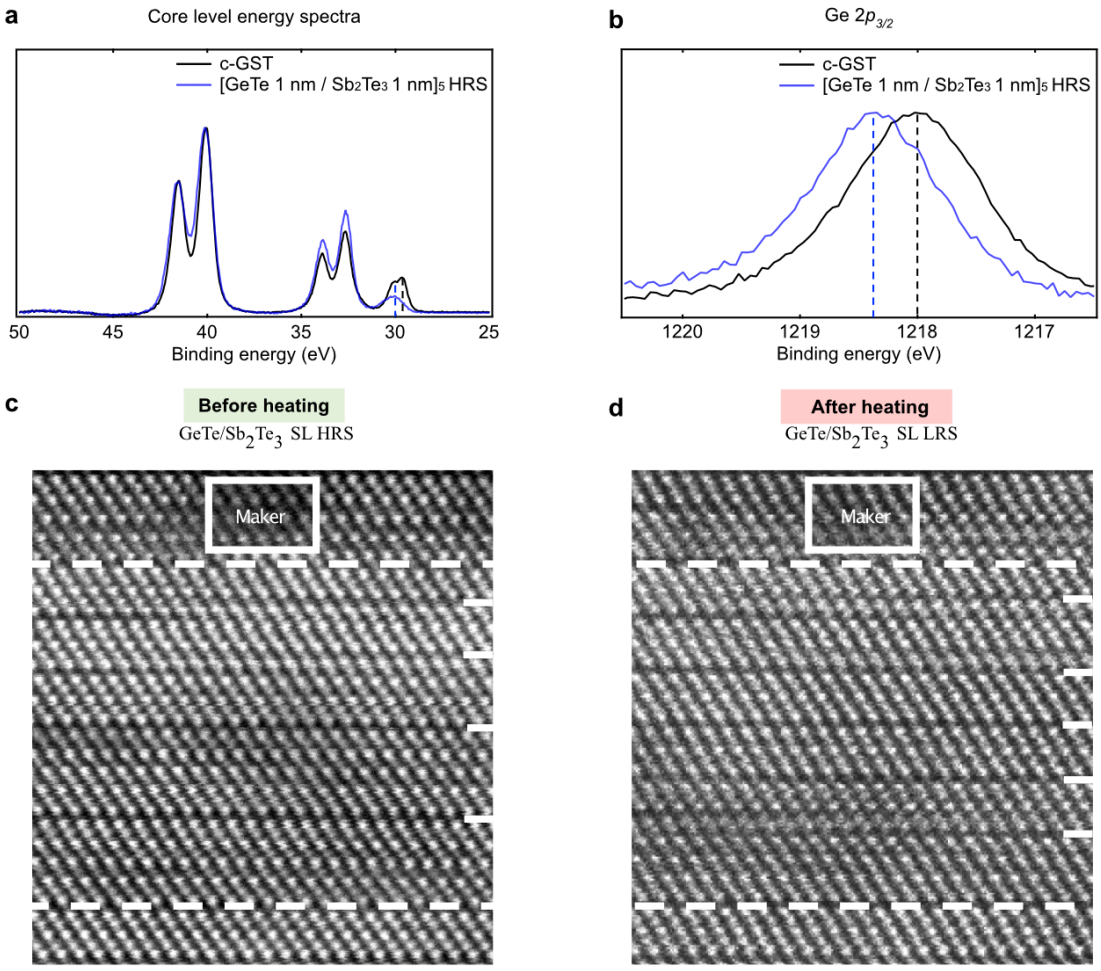

Fig. S6 | Local environments in [Sb_2Te_3 (1 nm)/ GeTe (1 nm)]$_5$/ Sb_2Te_3 10 nm SLs in the HRS and c-GST. a) Shallow core-level energy spectra of c-GST deposited by sputter and [Sb_2Te_3 (1 nm)/ GeTe (1 nm)]$_5$/ Sb_2Te_3 10 nm SLs in the HRS. b) Deep core-level spectra of Ge $2p_{3/2}$ in c-GST and [Sb_2Te_3 (1 nm)/ GeTe (1 nm)]$_5$/ Sb_2Te_3 10 nm SLs in the HRS. c) images taken before the phase transition marked through e-beam dosing. d) images taken after the annealing process. In the core-level energy state (Ge $2p_{3/2}$ spectra), the chemical binding energy of 29.7

eV (1218 eV) correspond to the octahedral ($Ge^{octahedral}$)[50], [53] structures, while 30.0 eV (1218.33 eV) conformed to the distorted octahedral ($Ge^{distorted\ octahedral}$)[54],[34] structures. As shown in Fig. S5a and 5b, the Ge local structure of c-GST is composed of an octahedral structure. Conversely, the HRS was a mixture of octahedral and distorted octahedral structures. Although the c-GST and HRS had similar structures in XRD results (Fig. S2), there were differences in the local structure around the Ge atoms.

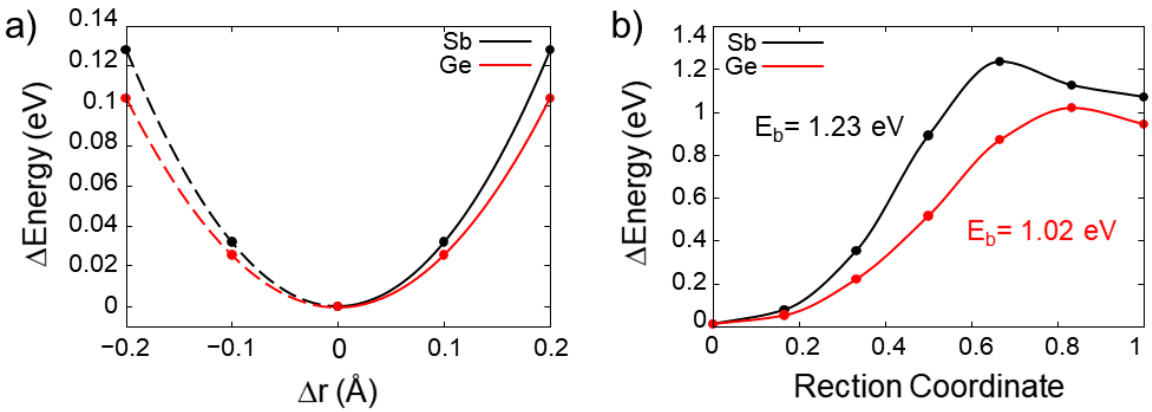

Fig. S7 | a) Energy curve with a small deviation of the atomic position of a single Ge (Sb) atom. Even though these two curves have similar curvatures, the attempt frequencies of the two atoms differ significantly because the atomic mass of the Sb atom is significantly heavier than that of the Ge atom. b) Minimum energy path during atom migration of a single Ge (Sb) atom from the cation layer to the neighboring vacancy layer.

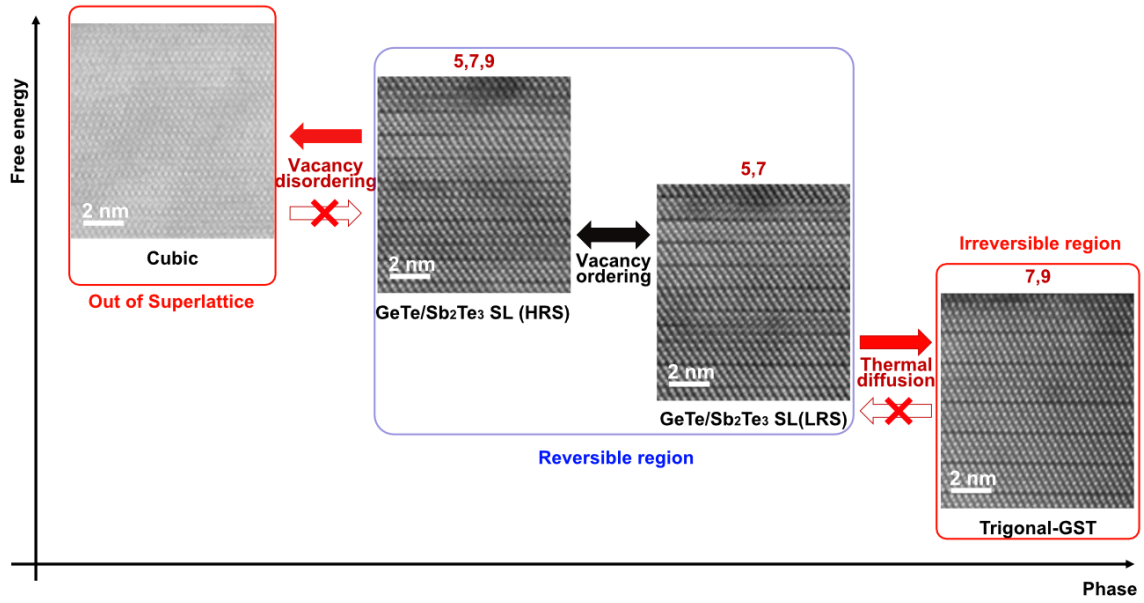

Fig. S8 | Schematic of the $GeTe/Sb_2Te_3$ SL phase versus free energy. Reversible transition between the HRS and LRS occurred through vacancy relocation. However, when thermal diffusion of GeTe into Sb_2Te_3 QLs occurred in the LRS above 300 °C, stable trigonal GST blocks were formed and reversible phase change became impossible.